Insights into the Enhanced Ceftazidime Hydrolysis by Ent385 AmpC β-lactamase from Multiscale Simulations

Anderson H. Lima[1,2*]; Marc W. van der Kamp[1*]

[1]School of Biochemistry, University of Bristol, University Walk, Bristol BS8 1TD, United Kingdom.

[2] Laboratório de Planejamento e Desenvolvimento de Fármacos, Instituto de Ciências Exatas e Naturais, Universidade Federal do Pará, Rua Augusto Corrêa, 01, 66075-110, Belém, Pará, Brasil.

ABSTRACT

The emergence of multidrug-resistant bacteria poses a significant threat to public health. Particularly, they are becoming increasingly resistant to β-lactam antibiotics, one of the most important drug classes for the treatment of bacterial infections. Ceftazidime-avibactam has shown promising activity against highly drug-resistant bacteria, including carbapenem-resistant Enterobacterales. However, an Ala294-Pro295 deletion in the Class C *E. cloacae* AmpC β-lactamase can confer reduced susceptibility to these agents. In this study, we investigated the molecular mechanisms underlying the enhanced hydrolysis of ceftazidime by *E. cloacae* Ent385 AmpC β-lactamase with the deletion using quantum mechanics/molecular mechanics (QM/MM) simulations. First, we used constant pH molecular dynamics simulations of the β-lactamase-ceftazidime acyl-enzyme complex to verify the likely protonation states, confirming Tyr150 primarily exists as a tyrosinate. We then used QM/MM (DFTB2/ff14SB) umbrella sampling to calculate reaction free energy barriers ($\Delta^{\ddagger}G$) for the deacylation step of cephalosporin hydrolysis. This reveals that Tyr150 (rather than the substrate) acts as the base. Importantly, the difference in $\Delta^{\ddagger}G$ between the canonical *E. cloacae* AmpC (P99) and the Ent385 variant was in very good agreement with the difference deduced from experimental kinetic data. Detailed analysis of the transition state ensembles, alongside additional simulations, show that the Ala294-Pro295 deletion allows the entrance of an additional water molecule, that helps stabilize the tetrahedral intermediate. Overall, our QM/MM simulations provide valuable insights into the reaction mechanism and reasons for enhanced ceftazidime breakdown. This can contribute to understand other reported Class C β-lactamase variants that confer reduced susceptibility to antibiotic treatment.

Introduction

The increase in bacteria developing resistance to multiple drugs is becoming a significant global health concern, threatening the effectiveness of conventional treatments. A particular concern is the growing resistance these pathogens are exhibiting against β-lactam antibiotics.[1] These drugs have been a strong defense against bacterial infections, yet their efficacy is increasingly threatened by the proliferation of resistance mechanisms, in particular those mediated by β-lactamases.[2] Over the past decades, combination therapy utilizing both a β-lactam antibiotic and a β-lactamase inhibitor has proven effective in managing resistance for the most difficult-to-treat infections. In particular, the combination of ceftazidime-avibactam (FDA approved in 2015) has emerged as a promising solution, with both classified as “critically important” by the WHO.[3] This combination exhibits strong activity against highly resistant bacteria, including those resistant to carbapenems.[4,5] However, the identification of variants of different β-lactamases has raised uncertainties regarding the future effectiveness of this treatment strategy. One particular case is the Ala294-Pro295 deletion found in the R2 loop of *E. cloacae*'s AmpC Ent385 β-lactamase, which increases the efficiency in hydrolyzing ceftazidime over 1,000 fold, compared to AmpC without this deletion, as found in AmpC P99.[6]

β-lactamases can be classified into four classes, A, B, C, and D (Ambler classification), according to their sequence similarity and catalytic mechanism of action.[7,8] Classes A, C and D function by a serine ester hydrolysis mechanism, whereas class B β-lactamases have zinc ions participating in catalysis.[8] Compared to the class A and D serine β-lactamases, the detailed hydrolysis mechanism of class C β-lactamases, also

known as AmpC, has remained unclear.[2] For the initial acylation step, Lys67 is believed to act as the general base to facilitate the nucleophilic attack by Ser64 on the carbonyl carbon of the β-lactam ring.[9] The proposed mechanism for deacylation, on the contrary, is extensively debated.[2,10] There are those suggesting that the β-lactam ring nitrogen is involved in the process (substrate-activated), and those proposing that proton transfers occur between Lys67, Tyr150, and the deacylating water (DW) without direct participation of the substrate (conjugate base), see Figure 1.

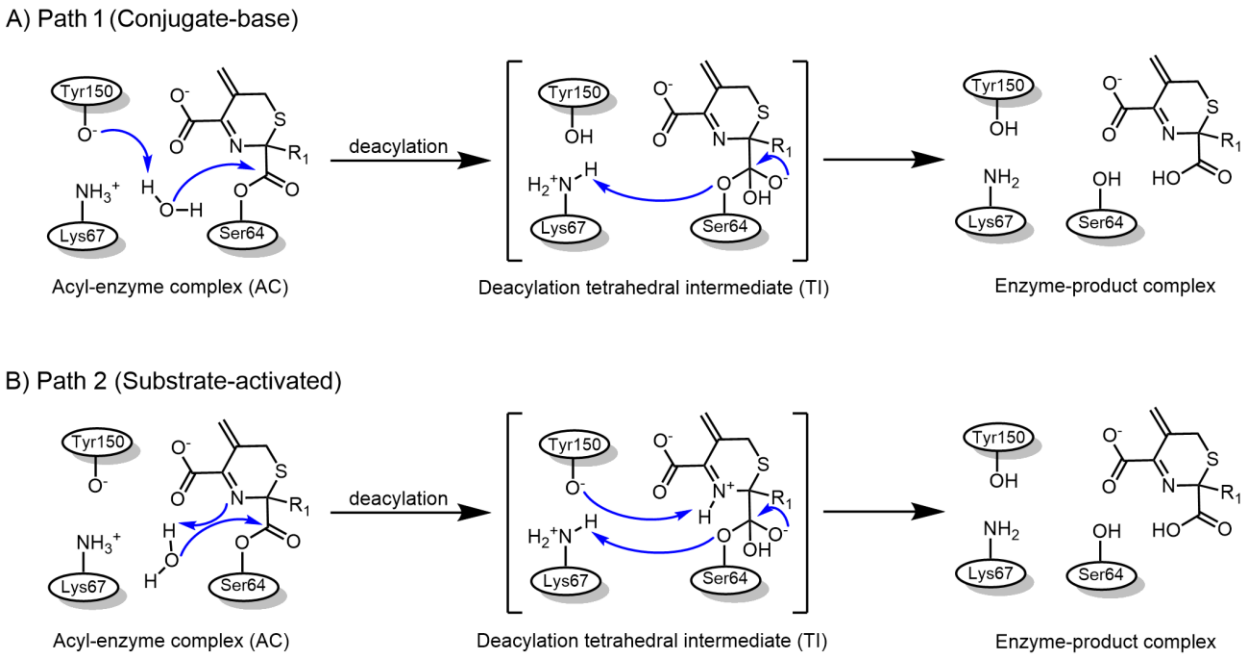

Figure 1. Possible mechanisms of acyl-enzyme deacylation in class C β-lactamases. A) Tyr150 (as tyrosinate) acting as "conjugate-base" to deprotonate the deacylating water (Path 1). B) "Substrate-activated" mechanism, with substrate N deprotonating the deacylating water (Path 2).

Tripathi and Nair (2016)[11] used QM/MM simulations to indicate that deprotonation of Tyr150 by transferring its proton to Lys67 is a critical step occurring prior to the activation of the DW molecule in the deacylation of the good substrate cephalotin. Thus, Tyr150 may function as the general base, while Lys67 can subsequently act as a general

acid, donating a proton to Ser64, which facilitates the regeneration of the free enzyme and the release of the hydrolyzed product.[12,13]

The alternative suggestion that the nitrogen in the β-lactam ring can act as the base ("substrate-assisted"), is supported by e.g. the high-resolution crystal structure of a tetrahedral intermediate model[14] and the fact that the absence or presence of the nitrogen can distinguish β-lactam inhibitors (i.e. no deacylation) from β-lactam substrates,[15] and consequently, distinguishing β-lactam antibiotics that are effective against AmpC-expressing bacteria from those to which these pathogens are resistant.[16] Thus, it has been suggested that this substrate nitrogen could act as a base, abstracting a proton from the DW. As a result, the mechanism of β-lactam hydrolysis in class C enzymes has remained unclear, and it is possible that either the "conjugate base" or "substrate-assisted" mechanism may dominate, depending on the enzyme-substrate combination.[2]

Here, we focused on deacylation of ceftazidime, with the main aim to unravel the molecular mechanism underlying the enhanced hydrolysis of ceftazidime by Ent385 AmpC β-lactamase, using quantum mechanics/molecular mechanics (QM/MM) molecular dynamics simulations following the reaction. First, we sought to determine the most likely deacylation mechanism for this important substrate, specifically identifying which base abstracts a proton from the DW during the ceftazidime hydrolysis process. Subsequently, we investigated the reasons behind the enhanced activity of Ent385 in comparison to the canonical P99 AmpC β-lactamase. Through our QM/MM simulations, we provide mechanistic details that explain experimentally-determined differences in kinetics, and thereby shed light on the origins of enhanced ceftazidime hydrolysis by the Ent385 AmpC β-lactamase.

Methods

Modeling acyl-enzyme structures

The crystal structure of AmpC Ent385 in complex with ceftazidime (AC state) was taken from the crystal structure, Protein Data Bank (PDB) code 6LC9.[6] The coordinates for AmpC P99 were taken from PDB code 4XUX (complex with a covalent boronic acid inhibitor, RPX-7009),[17] and ceftazidime was modeled in through alignment with 6LC9 (no clashes with protein residues occur). The parameters used for the ceftazidime adduct with Ser64 were the same as those described previously.[18] The AmpC Ent385 PDB file was used as the starting structure for constant pH MD (CpHMD) simulations, in Generalized Born implicit solvent (using the GB^{OBC} model, igb=2 in Amber20).[19] In this simulation, we titrated the important catalytic residues Lys67, Tyr150 and Lys315. Their protonation and deprotonation events were evaluated during simulations at a pH of 7.2. CpHMD simulations were carried out with the Amber20 program[20] employing the modified Amber ff10 force field and appropriate PBRadii set (mbondi2).[19]

The protonation states (including histidine tautomers) of the other residues were estimated using the H++ web server.[21] His198 was protonated on ND1, while His186, His193 and His313 were protonated on NE2. His39 and His210 are protonated on both ND1 and NE2. The corresponding histidines in AmpC P99 are protonated accordingly: His39 (ND1), His186 (both ND1 and NE2), His198 (NE2) and His313 (ND1). All other titratable residues are in their standard protonation states.

After determining the relevant protonation states of the titratable residues at pH 7.2 (used to determine steady-state kinetics by Kawai *et al.*),[6] MM MD simulations in explicit solvent were performed of the ceftazidime acylenzymes (AC) of AmpC Ent385

and P99. The system was solvated in a cubic box with TIP3P[22] water molecules, ensuring a minimum distance of 10 Å between the protein and the box edges. 4 Cl^- ions were added to neutralize the system by randomly replacing bulk water molecules. The protein was described using ff14SB.[23] For MM MD simulations, energy minimization, heating, and equilibration were performed (see SI for details). Production runs were performed in the NPT ensemble at 300 K and 1 atm using a 2 fs time step and the SHAKE algorithm. The default cut-off for direct-space non-bonded interactions was used, with Particle-Mesh Ewald used for long-range electrostatics. For each AC system, four independent simulations of 120 ns each were performed and analysed using CPPTRAJ.[24]

QM/MM simulations of ceftazidime deacylation

For QM/MM MD simulations, the self-consistent charge density functional tight-binding (SCC-DFTB, DFTB2) semi-empirical method[25,26] was used to describe the energy of the QM region while the remainder of the system was described by ff14SB[23] (protein, together with GAFF-based parameters for the ceftazidime adduct described previously[18]) and TIP3P (water). In these simulations, SHAKE was removed for the QM region only and a timestep of 1 fs was used, with other settings identical to the MM MD simulations. A total of 70 atoms were included in the QM region (Figure S1), which consisted of the entire ceftazidime (CTZ), the Ser64 and Tyr^-150 side chains (from Cβ), and the deacylating water (DW). The valences of the QM atoms at the QM/MM boundary were satisfied using the "link atom" method.[27] The charge and spin multiplicity for the QM region were defined as –3 and 1, respectively. DFTB2/ff14SB was used successfully previously to distinguish deacylation differences in Class A β-lactamases.[28–30]

Two-dimensional umbrella sampling QM/MM MD simulations were performed at the DFTB2/ff14SB level to compare two different proposed mechanisms: “conjugate-base” using Tyr150 (Path 1) and “substrate-activated” (Path 2), see Figure 1. Path 1 was followed starting from the AC complex using two Reaction Coordinates (RC_1 and RC_2) values to sample formation of the tetrahedral intermediate (TI). RC_1 describes the proton transfer from DW, and RC_2 the nucleophilic attack of DW on the acylenzyme carbonyl (RC_2 = d(O_{DW}-$C8_{CTZ}$)). In Path 1, RC_1 refers to the proton transfer between DW and Tyr150 as follows: RC_1 = d($O\eta_{Tyr150}$-H_{DW}) − d(O_{DW}-H_{DW}). In Path 2, RC_1 refers to proton transfer between DW and the substrate: RC_1 = d($N5_{CTZ}$-H_{DW}) − d(O_{DW}-H_{DW}).

The RCs were harmonically restrained to values ranging from −1.0 Å to 1.0 Å in RC_1 and from −3.4 Å to 1.4 Å in RC_2, with step sizes of 0.1 Å and a force constant of 100 kcal mol^{-1} $Å^{-2}$ and RC_2 was incremented further, using previous windows as starting points to sample all RC values. Then, 20 ps QM/MM MD production was run, with RC distances recorded every fs to build the 2D free energy profile employing the Weighted Histogram Analysis Method (WHAM),[31] using the wham2d code from the Grossfield lab,[32] where 80 bins were used for each reaction coordinate. Minimum free energy paths were then determined using MEPSA v1.4.[33] For the purpose of testing the accuracy of the DFTB2 method for the reaction, umbrella sampling was also run using the same protocol, but with the QM region extended to include the whole Ser64 residue and adjacent backbone atoms (Figure S1). Finally, comparison to DFT was done by exploring the potential energy surface, employing DFTB2/ff14SB and M06-2X single-point energy calculations with a large QM region (Figure S2; see further Results and Discussion).

Results and Discussion

Tyr150 is positioned to act as a base for deacylation of the ceftazidime acyl-enzyme complex in AmpC Ent385 β-lactamase

Throughout this work, we will use a standardized amino-acid numbering scheme that was recently developed for class C β-lactamases,[34] so that residue numbers of the key active site residues remain the same for AmpC P99 and AmpC Ent385 (despite the Ala294-Pro295 deletion in the latter, as shown in Figure S3). Before investigating the reaction, constant pH MD simulations in a generalized Born implicit solvent[19] were used to examine the likely protonation states of the catalytically important active site residues Lys67, Tyr150 and Lys315. The results shown in Table 1 were obtained with the ceftazidime acyl-enzyme complex of AmpC Ent385 (as taken from PDB ID 6LC9,[6] resolution 1.65 Å).

Table 1. Prediction of protonation states of important catalytic residues in AmpC Ent385 acyl-enzyme complex with ceftazidime from constant pH MD simulations.

Residue	Predicted pK_a apo (H++)	Predicted pK_a (CpHMD)	Average Fraction Protonated	Average Fraction Deprotonated
Lys67	>12.0	7.7	0.77	0.23
Tyr150	6.3	7.2	0.52	0.48
Lys315	> 12.0	∞	1.00	0.00

At pH 7.2, simulations revealed dynamic behavior in the protonation states of Lys67 and Tyr150, with multiple transitions observed in two independent runs. Lys67 remained predominantly protonated (~74–79%), while Tyr150 exhibited greater variability, shifting between protonated and deprotonated forms, visiting each with

approximately equal likelihood. In contrast, Lys315 remained fully protonated throughout. These protonation states are consistent with pKa predictions obtained using H^{++} [21] for the free enzyme (ceftazidime not included), see Table 1. These indicate that Tyr150 is predominantly deprotonated in the apo enzyme (predicted pKa 6.3), while both Lys67 and Lys315 are protonated. The dynamics of proton exchange, particularly for the Lys67/Tyr150 pair, was previously investigated by Tripathi and Nair for the *Enterobacter cloacae* 908R class C β-lactamase, who indicated that, among the various proposed protonation states of the apo protein, the most thermodynamically and kinetically stable configuration is where Tyr150 is deprotonated, while Lys67 and Lys315 remain protonated.[35] Their results showed that the stability of this protonation state is significantly affected by non-covalent binding of cephalothin. Here, a slight increase in the pK_a is found for Tyr150, with the protonated and deprotonated states present equally at pH 7.2, and a larger decrease in pK_a for Lys67. Tooke *et al.* (2019)[2] emphasize the balance between the roles of Tyr150 and Lys67 in the acylation and deacylation steps. Although the deprotonation of Tyr150 by Lys67 is not a rate-limiting step, it has been considered critical for the deacylation reaction, occurring before the activation of the catalytic water molecule.[11]

Previous studies by Adediran and Pratt (1999)[36] and Díaz et al (2006)[9] explored the possible protonation states of the Lys67/Tyr150 pair in class C β-lactamases. Our CpHMD simulations indicate that two protonation states are accessible (with similar likelihood) in the ceftazidime acyl-enzyme complex with AmpC Ent385. The protonation state Lys67^{+}/Tyr150^{-}/Lys315^{+} is referred to as the Tyrosinate configuration, while Lys67/Tyr150/Lys315^{+} is referred to as the Tyrosine configuration. We performed

conventional MM MD simulations in explicit solvent on both configurations, showing that the protonation states of Lys67 and Tyr150 have a significant impact on the detailed conformation of the acyl-enzyme (AC) ensemble. The results suggest that the configuration with Tyr150 negatively charged is more favorable for deacylation compared to neutral Tyr150. In the former Tyrosinate configuration, a water molecule is more frequently located in the optimal position for deacylation: a higher density of water molecules is observed around the electrophilic carbon of ceftazidime, particularly within the 3.5–4.0 Å range (Figure S4). Hydrogen bond analysis for the AC complex of AmpC Ent385 with ceftazidime indicates that when Lys67 is neutral, it predominantly forms a hydrogen bond with Tyr112 (Figure S5). It has been reported that the orientation of Tyr150 can be influenced by hydrophobic interactions with the Tyr112 side chain, with correlated movement observed between these residues.[9] Additionally, Lys315 was found to frequently interact with Tyr150, contributing to the stability of the tyrosinate. These results highlight the role of Lys67 in the deacylation process. When Lys67 is in its neutral state and accepting a hydrogen bond from Tyr112, it is not properly oriented to act as a base for abstracting a proton from the deacylating water during its nucleophilic attack. In contrast, with Lys67 protonated, Tyr150 (in its tyrosinate state) is well-positioned to fulfill this role, emphasizing the likely importance of a coordinated role of Lys67 and Tyr150 in the deacylation mechanism. Finally, after the formation of the deacylation tetrahedral intermediate, Lys67 (in its protonated form) can transfer a proton to Ser64, restoring the active site of AmpC Ent385 for subsequent hydrolysis cycles (Figure 1). Based on these observations, the Tyrosinate configuration can be considered the most relevant for

deacylation activity and was thus chosen as the starting point for the subsequent QM/MM reaction simulations.

Ceftazidime deacylation in E. cloacae AmpC involves Tyr150 acting as a base

We performed QM/MM (DFTB2/ff14SB) umbrella sampling simulations to compare the two different proposed ceftazidime deacylation mechanisms shown in Figure 1, in AmpC Ent385. The aim of this was to evaluate which base most likely abstracts the proton from the deacylating water (DW), and whether this deprotonation of DW is concerted with its nucleophilic attack on the acyl carbon. Reaction-free energy barriers ($\Delta^{\ddagger}G$) for the deacylation step of ceftazidime hydrolysis indicate that the "conjugate base" mechanism with Tyr150 acting as the base (Path 1) is favored by 7.2 kcal/mol over the "substrate-assisted" mechanism (Path 2). Thus, according to our simulations, Tyr150 acts as a base in the ceftazidime deacylating reaction. The minimum free energy pathway (Figure 2 and Figure S2) shows that proton transfer and nucleophilic attack occur in a concerted fashion. Although the transition state is located approximately at the same point on the free energy surface for both Path1 and Path 2, it is observed that in Path1, the network of hydrogen bond interactions is more favorable for stabilizing the intermediates than in Path 2. During the TI formation in Path 1, the OH group added to the electrophilic carbon of ceftazidime forms a stabilising hydrogen bond with the hydroxyl group of Tyr150, where Tyr150 acts as a hydrogen bond donor. In contrast, in Path 2, this OH group potentially serves as a third hydrogen bond donor to the oxyanion of Tyr150, which is already stabilised by interactions with Lys67 and Lys315. This difference in hydrogen bonding likely contributes to the increased stability of the TI and also the lower activation energy

observed in Path 1 compared to Path 2. We further measured the distance between the oxyanion of Tyr150 and the protonated substrate nitrogen in the TI obtained from Path 2 (4.35 ± 0.19 Å). This relatively long distance suggests that regeneration of the active site of AmpC Ent385 may come at an additional energy cost. Specifically, Tyr150 would need to capture the proton from the nitrogen of ceftazidime, likely occurring after TI formation, either as the TI collapses or immediately following product formation.

Next, we compared the calculated free energy barrier of Path 1 with the experimentally derived rate. Based on a k_{cat} of 25.8 s^{-1},[6] and the Eyring equation, the free energy barrier ($\Delta^{\ddagger}G$) should have an upper limit of 15.7 kcal/mol. Notably, the $\Delta^{\ddagger}G$ from our initial DFTB2/ff14SB umbrella sampling is higher, by 3.6 kcal/mol. When performing umbrella sampling simulations with an increased QM region (now including the main chain nitrogen of Ser64, which contributes to oxyanion stabilisation), this overestimation is removed, resulting in good agreement with the barrier derived from the experimental rate (16.0 kcal/mol; Figure S2A). Further, potential energy profile determination indicates that QM/MM energies using DFTB2 and DFT (M06-2X/def2-SVP) are similar (Figure S2C). Therefore, the overestimation of the barrier observed with the smaller QM region is due to the inacurrate oxanion hole stabilisation rather than shortcomings of the DFTB2 method for this particular reaction. Together, this indicates that Path 1, with Tyr150 acting as the base to abstract the proton from DW, is consistent with experimental kinetics for ceftazidime hydrolysis in Ent385. While DFTB2 tends to underestimate the energy barrier for deacylation in class A and D serine β-lactamases,[28,37] this is not observed here, with Tyr150 acting as the base.

QM/MM simulations of deacylation accurately capture the enhanced ceftazidime hydrolysis activity of AmpC Ent385

The increase in the catalytic efficiency of class C β-lactamases against extended-spectrum cephalosporins is mainly due to missense mutations that result in amino acid substitutions and/or deletions.[10] In the particular case of AmpC Ent385, the deletion of residues 294 and 295 causes structural changes to the R2-loop (residues 286 to 310). Nevertheless, the positioning of the important motifs ^{64}SXSK, ^{150}YXN, and ^{315}KTG are conserved between the two variants. Our simulations can shed light on the origins of enhanced ceftazidime hydrolysis by the Ent385 AmpC β-lactamase. The difference in the predicted $\Delta^{\ddagger}G$ between the canonical *E. cloacae* AmpC P99 and the AmpC Ent385 variant is 3.3 kcal/mol (19.3 ± 0.8 kcal/mol vs. 22.6 ± 1.0 kcal/mol, respectively) is in good agreement with the expected difference deduced from experimental kinetic data. When Ala294-Pro295 is reinserted into AmpC Ent385, this leads to a significant reduction in rate (k_{cat} of 0.03 s^{-1} vs. 25.8 s^{-1}),[6] indicating a $\Delta\Delta^{\ddagger}G$ of 3.9 kcal/mol. Similarly, deletion of Ala294-Pro295 from AmpC P99 leads to an increase in rate (from 0.0061 s^{-1} to 0.028 s^{-1}, corresponding to a $\Delta\Delta^{\ddagger}G$ of 0.9 kcal/mol) (A direct comparison of the rates of AmpEnt385 and AmpC P99 is difficult because the k_{cat} values are obtained by different labs and protocols). Together with the good agreement between the calculated barriers (with the larger QM region) and those inferred from k_{cat} values, this indicates that deacylation is likely rate-limiting for ceftazidime hydrolysis in AmpC Ent385 and P99. Tripathi and Nair previously found that acylation was more likely to be rate-limiting in the hydrolysis of the good substrate cephalotin (in *Enterobacter cloacae* 908R class C β-lactamase), but the rate-limiting step can be different for different enzyme-substrate combinations.[2,35]

The crystal structures of ceftazidime and a boronic acid transition-state analogue inhibitor in complex with AmpC from *Escherichia coli* suggested how ceftazidime (and other later generation cephalosporins) are not easily hydrolyzed by class C β-lactamases.[38] Overall, their R1 moiety results in unfavourable interactions with the enzyme, particularly involving residues Val211 and Tyr221. Here, we compare the structures of the AC complexes in AmpC Ent385 and P99 by superimposing their Cα atoms. Although the structural similarity in the protein backbone was high (Cα RMSD of 0.7 Å), a notable structural difference was observed at the C4 carboxylate substituent of the β-lactam ring (Figure 2D). Apart from the Ala294-Pro295 deletion, AmpC Ent385 also features a range of substitutions compared to AmpC P99 (Figure S3), including a substitution at position 289, where Ser in P99 is replaced by Asn in Ent385. Residue 289 is not conserved among class C β-lactamases,[10] and Asn289 is found in several clinically relevant AmpC enzymes such as FOX-1 (*Klebsiella pneumoniae*)[39] and EC-1 (*Escherichia coli*)[40]. It has been indicated to play an important role in interactions with inhibitors,[41] and thus likely can influence acyl-enzyme binding. In AmpC Ent385, the Ala294-Pro295 deletion results in Leu293 moving away from the active site, removing a potential steric clash with the methylene group and thus providing space for Asn289 to interact with the C4 carboxylate group of ceftazidime. The altered interaction network compared to AmpC P99 that is facilitated by these structural changes, suggests that Ent385 has adapted to better accommodate the ceftazidime acyl-enzyme, which in turn can be related to enhancing its hydrolytic activity for this substrate.

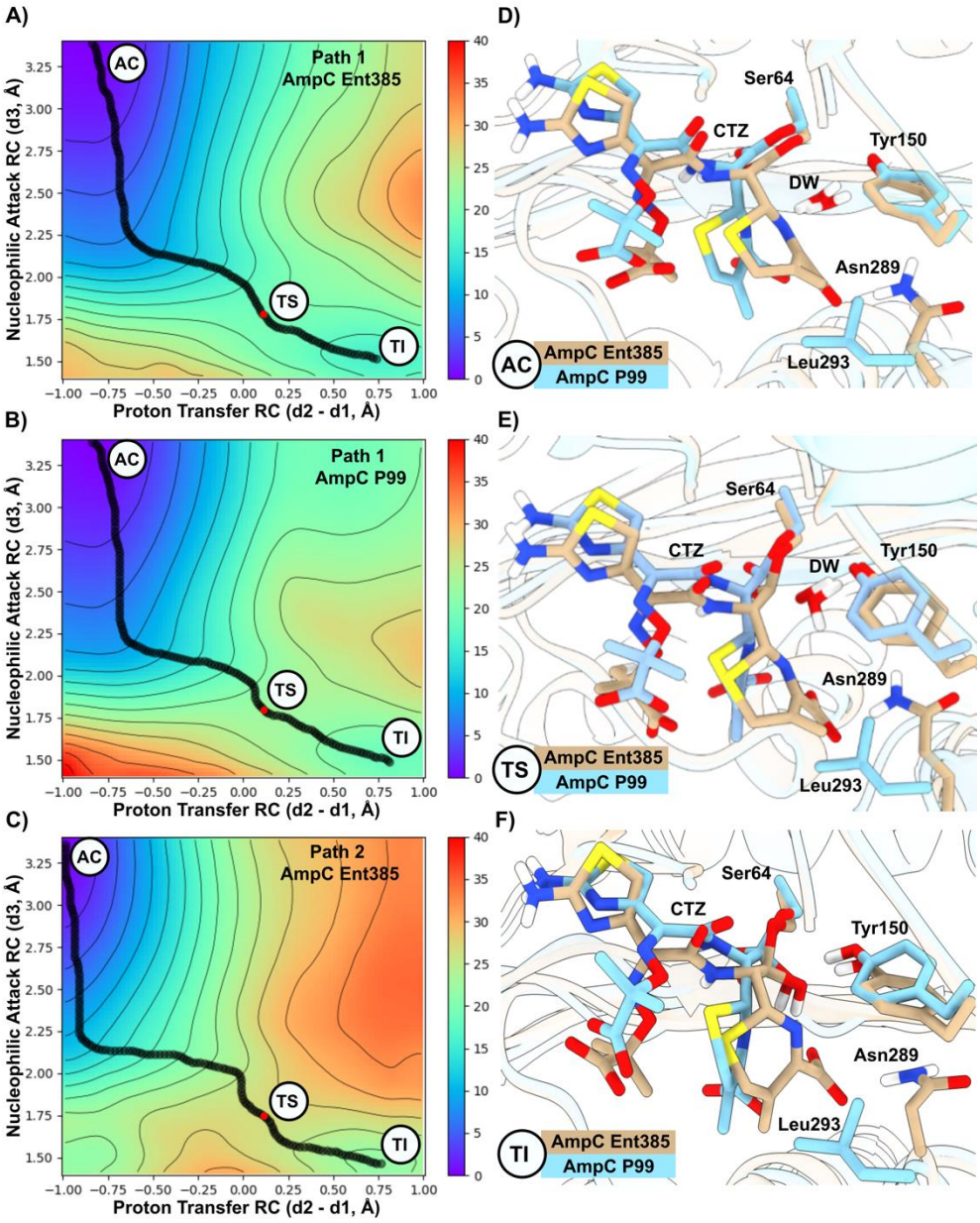

Figure 2. QM/MM reaction simulations of ceftazidime deacylation in Ent385 and P99 AmpC. (A-C) Two-dimensional free energy surfaces for ceftazidime hydrolysis considering the conjugate-base mechanism (Path 1, panels A and B) and substrate-activated mechanism (Path 2, panel C), obtained from umbrella sampling at the DFTB2/ff14SB level. AC is Acyl-Enzyme, TS the approximate transition state (red dots), and TI the Tetrahedral Intermediate state. (D-F) Representative (as determined by clustering analysis on RMSD of ceftazidime) AC, TS and TI structures of AmpC P99 (cyan) and AmpC Ent385 (tan). Non-polar hydrogens have been omitted for clarity.

Examination of transition state ensembles for AmpC Ent385 compared to the 'parent' P99 suggests that the Ent385 active site conformation is more conducive to deacylation, especially through the interaction of the (former) β-lactam ring nitrogen and the deacylating water (Figure S7). The resulting hydrogen bond donation by DW to this nitrogen is expected to increase the nucleophilicity of DW, similar to what was found for DW hydrogen bond donation to carbapenem acylenzymes (6-hydroxyethyl moiety) in OXA-48.[42] Thus, the repositioning of residue Leu293 in AmpC Ent385 allows for better accommodation of the ceftazidime acylenzyme in a reactive position, which in AmpC P99 is unlikely to occur due to steric hindrance of the methylene group with Leu293. Interaction fingerprint analysis indicates that Leu293 forms more hydrophobic interactions with ceftazidime in AmpC P99 compared to AmpC Ent385 (Figure S8). The importance of this residue was previously assessed using site-directed mutagenesis, with 15 different replacements for Leu293 tested.[43] Only the Leu293Pro mutant (expected to lead to some restructuring of the R2 loop) exhibited increased catalytic efficiencies for cefepime and ceftazidime, likely contributing to higher MICs for these antibiotics. Interaction fingerprint analysis also highlights differences in interactions with Arg203, Asn/Ser289 and Thr316. Particularly, Asn289 in AmpC Ent385 contributes to holding the C4 carboxylate group close to the reaction center.

Additional oxyanion stabilization by a water molecule causes enhanced ceftazidime hydrolysis in AmpC Ent385

Further analysis of the reaction simulations revealed a difference in active site hydration during the deacylation between AmpC Ent385 and P99. In particular, an

additional water molecule was observed to enter the oxyanion hole of the Ent385 active site (Figure 3), offering additional stabilization of the emerging oxyanion in the transition state ensemble (and beyond), thus potentially enhancing catalytic efficiency. Initially, in the AC state, this water molecule forms a bridge between Ser318-OH and the C4 substituent carboxylate group. As the reaction progresses, it then enters the oxyanion hole. This bridging water is observed in the experimentally determined structure of AmpC Ent385, whereas it is absent in that of AmpC P99 (Figure 3). In the latter, Ser318-OH and the C4 caroxylate are therefore closer together. Water molecules in β-lactamases have been shown to play critical roles in catalysis and can exchange rapidly with bulk solvent. An early MD study on a class A β-lactamase already suggested that active site water molecules, including the "hydrolytic" and "oxyanion hole" waters, exchange with the bulk solvent at a rate faster than the catalytic process.[44] In more recent work, it was shown that limiting the hydration of the general base likely plays a crucial role in determining deacylation efficiency in clinically relevant OXA-48-like β-lactamases.[18,42]

Here, we first investigated the difference of the interactions between Ser318 and the ceftazidime carboxylate in our MM MD simulations of the acyl-enzyme states of AmpC Ent385 and P99. We monitored the distance between the Ser318 hydroxyl oxygen and the C4 carboxylate oxygen in frames classified as 'reactive conformations', i.e., those with the distance between the oxygen of the deacylating water and the electrophilic carbon less than 3.5 Å, and with Tyr150 Oη within 2.5 Å. In AmpC P99, the distance is predominantly < 3 Å (as in the crystal structure), suggesting that the presence of a bridging water molecule between Ser318 and the carboxylate unlikely (Figure S9). Even when the distance between Ser318 and the C4 carboxylate oxygen is more than 3.5 Å,

Arg349 can take the position between them, whereas this is usually taken by the additional water molecule in AmpC Ent385 (consistent with its crystal structure). QM/MM simulations of the AC, TS and TI states starting from the same (AC-based) enzyme conformation (where the water bridges Ser318 and the C4 carboxylate) indicate that movement of the water from the Ser318-carboxylate bridging position to the oxyanion hole occurs only when negative charge is accumulating on the oxyanion (in TS and TI), and this movement is fast (~ps timescale, Figure S10).

To test whether the presence of the additional “oxyanion hole” water molecule in the transition state of ceftazidime deacylation by AmpC Ent385 is responsible for a lower energy barrier for deacylation, we compared reaction simulations with and without this additional water molecule, in both AmpC P99 and Ent385. We identified some cases in the AmpC P99 acyl-enzyme MM MD simulations where a bridging water molecule was present. For both variants, we thus selected two 'reactive conformation' snapshots that included the bridging water molecule (as observed in the crystal structure of Ent385, PDB ID: 6LC9), and two snapshots without this water molecule, where Ser318 directly interacted with the C4 carboxylate of ceftazidime. All these snapshots (4 for each system) were then used as the starting point for QM/MM reaction simulations (using the same protocols used before). The average free energy barriers from these reaction simulations (Figure 3) clearly indicate that the additional water molecule, which moves to the oxyanion hole during the reaction, causes a significant reduction in the activation energy (by stabilizing the emerging oxyanion in the AmpC-ceftazidime TS complex). For AmpC Ent385, where the bridging water is expected in the acylenzyme (based on our MM MD simulations and the crystal structure), the reduction in barrier due to the additional water-

oxyanion hydrogen bond is 4.4 kcal/mol. For AmpC P99, where no bridging water is expected, the barrier is reduced by a similar amount.

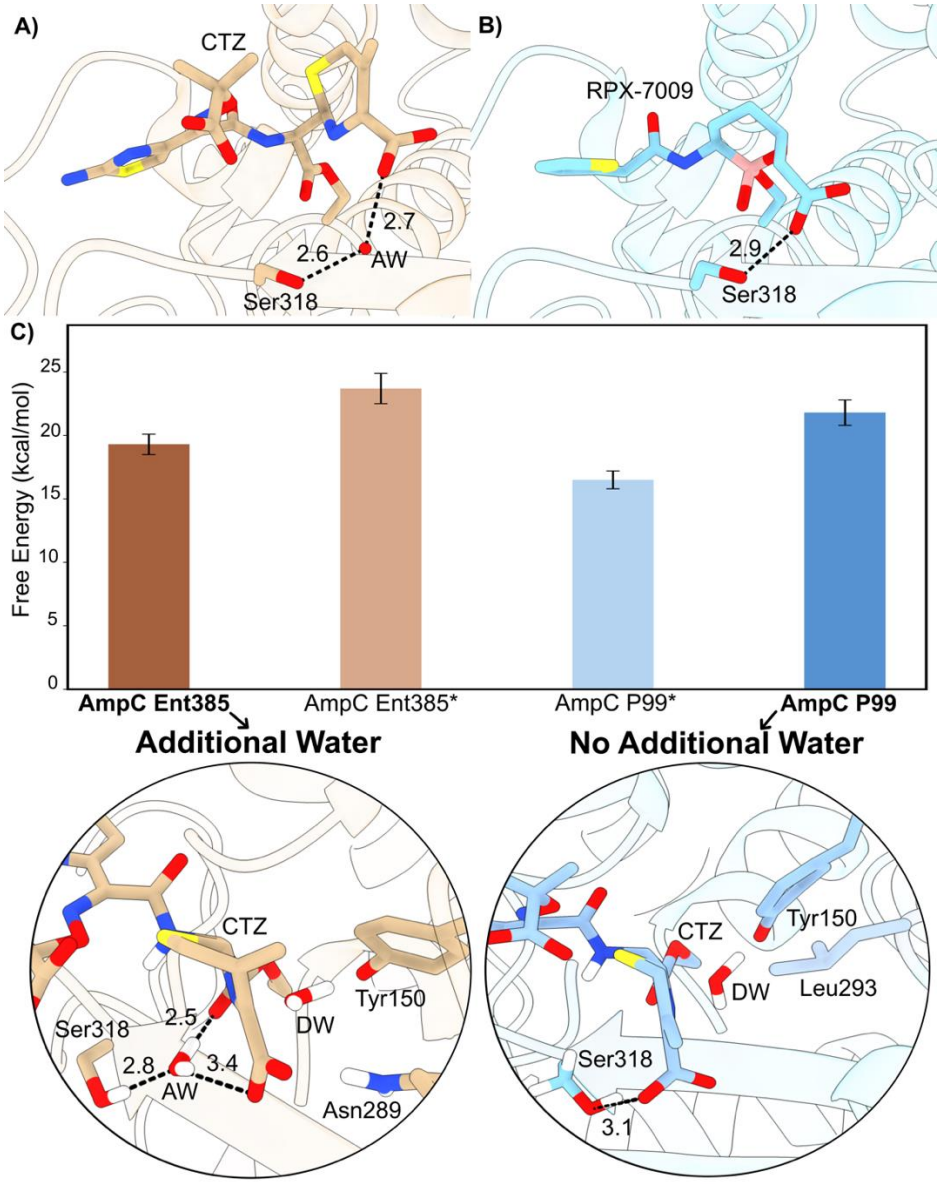

Figure 3. Free energy barriers and representative transition state structures from umbrella sampling simulations for AmpC Ent385 and P99 from different active site conformations. For each bar, the average free energy barrier from 3 (likely conformations) or 2 (unlikely conformations) QM/MM umbrella sampling simulations is shown (with the error bar indicating the standard deviation). *Represents unlikely conformations of each variant.

This analysis indicates that the additional water molecule is crucial for stabilizing the transition state in Ent385, thereby lowering the activation energy and enhancing catalytic efficiency. Only when the additional water is present in the transition state in Ent385, and *not* in P99, does the calculated difference in barrier correctly indicate the expected difference in ceftazidime hydrolysis kinetics.

Conclusions

Our study has unveiled the detailed mechanism underlying the enhanced hydrolysis of ceftazidime by the Ent385 variant of AmpC β-lactamase. Constant pH simulations show that Tyr150 can be present as a tyrosinate in the ceftazidime acylenzyme (at no free energy cost), and QM/MM umbrella sampling simulations clearly indicate that Tyr150 is acting as a base in the deacylation reaction. Furthermore, these QM/MM reaction simulations capture a significant difference in $\Delta^{\ddagger}G$ between the canonical *E. cloacae* AmpC (P99) and the Ent385 variant for ceftazidime deacylation, which aligns well with available experimental data. Transition state structure analysis revealed that the active site conformation in the Ent385 variant is better optimized for deacylation due to the Ala294-Pro295 deletion (as well as the Ser289Asn mutation). One of the consequences of this is that a water molecule can contribute to oxyanion stabilization in Ent385. Our simulations highlighted the crucial role of this extra water molecule in stabilizing the transition state in this variant, leading to increased ceftazidime hydrolysis activity. This information may aid the design of more effective inhibitors. As bacteria continually evolve and new beta-lactamase variants that confer resistance

emerge, understanding these detailed mechanisms is essential for developing advanced strategies to combat antibiotic resistance and improve treatment efficacy.

Supporting Information statement

Details of molecular mechanics molecular dynamics simulations, description of QM regions in QM/MM simulations (Figure S1), free and potential energy surfaces, including DFT corrected energies (Figure S2), AmpC Ent385 vs. AmpC P99 sequence alignment (Figure S3), histograms of key interaction distances (Figure S4-S5, S7 and S9), and structural representations of reaction intermediates in Path 2 (Figure S6). We also provide interaction fingerprints for ceftazidime in the AmpC P99 and Ent385 acyl-enzymes (Figure S8), and distances relevant to catalytic activity (Figure S10).

Author Contributions

The study was designed and the manuscript was written by both authors. A.H.L performed all simulations, with guidance from M.W.vdK. Both authors analyzed the results.

Funding

A.H.L and M.W.vdK. thank the Royal Society for support (Newton International Fellowship to A.H.L, NIF\R1\221443). This work was conducted using the computational facilities of the Advanced Computing Research Centre, University of Bristol.

References

(1) Mora-Ochomogo, M.; Lohans, C. T. β-Lactam Antibiotic Targets and Resistance Mechanisms: From Covalent Inhibitors to Substrates. *RSC Med. Chem.* **2021**, *12* (10), 1623–1639. https://doi.org/10.1039/d1md00200g.

(2) Tooke, C. L.; Hinchliffe, P.; Bragginton, E. C.; Colenso, C. K.; Hirvonen, V. H. A.; Takebayashi, Y.; Spencer, J. β-Lactamases and β-Lactamase Inhibitors in the 21st Century. *J. Mol. Biol.* **2019**, *431* (18), 3472–3500. https://doi.org/10.1016/j.jmb.2019.04.002.

(3) García-Castro, M.; Sarabia, F.; Díaz-Morilla, A.; López-Romero, J. M. Approved Antibacterial Drugs in the Last 10 Years: From the Bench to the Clinic. *Explor. Drug Sci.* **2023**, 180–209. https://doi.org/10.37349/eds.2023.00013.

(4) Fiore, M.; Alfieri, A.; Di Franco, S.; Pace, M. C.; Simeon, V.; Ingoglia, G.; Cortegiani, A. Ceftazidime-Avibactam Combination Therapy Compared to Ceftazidime-Avibactam Monotherapy for the Treatment of Severe Infections Due to Carbapenem-Resistant Pathogens: A Systematic Review and Network Meta-Analysis. *Antibiotics* **2020**, *9* (7), 388. https://doi.org/10.3390/antibiotics9070388.

(5) Hakeam, H. A.; Alsahli, H.; Albabtain, L.; Alassaf, S.; Al Duhailib, Z.; Althawadi, S. Effectiveness of Ceftazidime–Avibactam versus Colistin in Treating Carbapenem-Resistant Enterobacteriaceae Bacteremia. *Int. J. Infect. Dis.* **2021**, *109*, 1–7. https://doi.org/10.1016/j.ijid.2021.05.079.

(6) Kawai, A.; McElheny, C. L.; Iovleva, A.; Kline, E. G.; Sluis-Cremer, N.; Shields, R. K.; Doi, Y. Structural Basis of Reduced Susceptibility to Ceftazidime- Avibactam and Cefiderocol in Enterobacter Cloacae Due to AmpC R2 Loop Deletion. *Antimicrob. Agents Chemother.* **2020**, *64* (7). https://doi.org/10.1128/AAC.00198-20.

(7) Ambler, R. P. The Structure of Beta-Lactamases. *Philos. Trans. R. Soc. Lond. B. Biol. Sci.* **1980**, *289* (1036), 321–331. https://doi.org/10.1098/rstb.1980.0049.

(8) Hall, B. G.; Barlow, M. Revised Ambler Classification of β-Lactamases. *J. Antimicrob. Chemother.* **2005**, *55* (6), 1050–1051. https://doi.org/10.1093/jac/dki130.

(9) Díaz, N.; Suárez, D.; Sordo, T. L. Molecular Dynamics Simulations of Class C β-Lactamase from Citrobacter Freundii : Insights into the Base Catalyst for Acylation. *Biochemistry* **2006**, *45* (2), 439–451. https://doi.org/10.1021/bi051600j.

(10) Philippon, A.; Arlet, G.; Labia, R.; Iorga, B. I. Class C β-Lactamases: Molecular Characteristics. *Clin. Microbiol. Rev.* **2022**, *35* (3), e0015021. https://doi.org/10.1128/cmr.00150-21.

(11) Tripathi, R.; Nair, N. N. Deacylation Mechanism and Kinetics of Acyl-Enzyme Complex of Class C β-Lactamase and Cephalothin. *J. Phys. Chem. B* **2016**, *120* (10), 2681–2690. https://doi.org/10.1021/acs.jpcb.5b11623.

(12) Chen, Y.; McReynolds, A.; Shoichet, B. K. Re-examining the Role of Lys67 in Class C β-Lactamase Catalysis. *Protein Sci.* **2009**, *18* (3), 662–669. https://doi.org/10.1002/pro.60.

(13) Beadle, B. M.; Trehan, I.; Focia, P. J.; Shoichet, B. K. Structural Milestones in the Reaction Pathway of an Amide Hydrolase. *Structure* **2002**, *10* (3), 413–424. https://doi.org/10.1016/S0969-2126(02)00725-6.

(14) Chen, Y.; Minasov, G.; Roth, T. A.; Prati, F.; Shoichet, B. K. The Deacylation Mechanism of AmpC β-Lactamase at Ultrahigh Resolution. *J. Am. Chem. Soc.* **2006**, *128* (9), 2970–2976. https://doi.org/10.1021/ja056806m.

(15) Bulychev, A.; Massova, I.; Miyashita, K.; Mobashery, S. Nuances of Mechanisms and Their Implications for Evolution of the Versatile β-Lactamase Activity: From Biosynthetic Enzymes to Drug Resistance Factors. *J. Am. Chem. Soc.* **1997**, *119* (33), 7619–7625. https://doi.org/10.1021/ja963708f.

(16) Patera, A.; Blaszczak, L. C.; Shoichet, B. K. Crystal Structures of Substrate and Inhibitor Complexes with AmpC β-Lactamase: Possible Implications for Substrate-Assisted Catalysis. *J. Am. Chem. Soc.* **2000**, *122* (43), 10504–10512. https://doi.org/10.1021/ja001676x.

(17) Hecker, S. J.; Reddy, K. R.; Totrov, M.; Hirst, G. C.; Lomovskaya, O.; Griffith, D. C.; King, P.; Tsivkovski, R.; Sun, D.; Sabet, M.; Tarazi, Z.; Clifton, M. C.; Atkins, K.; Raymond, A.; Potts, K. T.; Abendroth, J.; Boyer, S. H.; Loutit, J. S.; Morgan, E. E.; Durso, S.; Dudley, M. N. Discovery of a Cyclic Boronic Acid β-Lactamase Inhibitor (RPX7009) with Utility vs Class A Serine Carbapenemases. *J. Med. Chem.* **2015**, *58* (9), 3682–3692. https://doi.org/10.1021/acs.jmedchem.5b00127.

(18) Hirvonen, V. H. A.; Mulholland, A. J.; Spencer, J.; van der Kamp, M. W. Small Changes in Hydration Determine Cephalosporinase Activity of OXA-48 β-Lactamases. *ACS Catal.* **2020**, *10* (11), 6188–6196. https://doi.org/10.1021/acscatal.0c00596.

(19) Mongan, J.; Case, D. A.; McCammon, J. A. Constant PH Molecular Dynamics in Generalized Born Implicit Solvent. *J. Comput. Chem.* **2004**, *25* (16), 2038–2048. https://doi.org/https://doi.org/10.1002/jcc.20139.

(20) Case, D. A.; Aktulga, H. M.; Belfon, K.; Ben-Shalom, I. Y.; Brozell, S. R.; Cerutti, D. S.; Cheatham, T. E.; Cisneros, G. A.; Cruzeiro, V. W. D.; Darden, T. A.; Duke, R. E.; Giambasu, G.; Gilson, M. K.; Gohlke, H.; Goetz, A. W.; Harris, R.; Izadi, S.;

Izmailov, S. A.; Jin, C.; Ka, K. No Title. University of California: San Francisco 2021. https://ambermd.org/index.php.

(21) Anandakrishnan, R.; Aguilar, B.; Onufriev, A. V. H++ 3.0: Automating PK Prediction and the Preparation of Biomolecular Structures for Atomistic Molecular Modeling and Simulations. *Nucleic Acids Res.* **2012**, *40* (W1), W537–W541. https://doi.org/10.1093/nar/gks375.

(22) Jorgensen, W. L.; Chandrasekhar, J.; Madura, J. D.; Impey, R. W.; Klein, M. L. Comparison of Simple Potential Functions for Simulating Liquid Water. *J. Chem. Phys.* **1983**, *79* (2), 926–935. https://doi.org/10.1063/1.445869.

(23) Maier, J. A.; Martinez, C.; Kasavajhala, K.; Wickstrom, L.; Hauser, K. E.; Simmerling, C. Ff14SB: Improving the Accuracy of Protein Side Chain and Backbone Parameters from Ff99SB. *J. Chem. Theory Comput.* **2015**, *11* (8), 3696–3713. https://doi.org/10.1021/acs.jctc.5b00255.

(24) Roe, D. R.; Cheatham, T. E. PTRAJ and CPPTRAJ: Software for Processing and Analysis of Molecular Dynamics Trajectory Data. *J. Chem. Theory Comput.* **2013**, *9* (7), 3084–3095. https://doi.org/10.1021/ct400341p.

(25) Seabra, G. D. M.; Walker, R. C.; Elstner, M.; Case, D. A.; Roitberg, A. E. Implementation of the SCC-DFTB Method for Hybrid QM/MM Simulations within the Amber Molecular Dynamics Package. *J. Phys. Chem. A* **2007**, *111* (26), 5655–5664. https://doi.org/10.1021/jp070071l.

(26) Elstner, M.; Porezag, D.; Jungnickel, G.; Elsner, J.; Haugk, M.; Frauenheim, T. Self-Consistent-Charge Density-Functional Tight-Binding Method for Simulations of Complex Materials Properties. *Phys. Rev. B - Condens. Matter Mater. Phys.* **1998**, *58* (11), 7260–7268. https://doi.org/10.1103/PhysRevB.58.7260.

(27) Singh, U. C.; Kollman, P. A. A Combined Ab Initio Quantum Mechanical and Molecular Mechanical Method for Carrying out Simulations on Complex Molecular Systems: Applications to the CH3Cl + Cl− Exchange Reaction and Gas Phase Protonation of Polyethers. *J. Comput. Chem.* **1986**, *7* (6), 718–730. https://doi.org/10.1002/jcc.540070604.

(28) Chudyk, E. I.; Limb, M. A. L.; Jones, C.; Spencer, J.; van der Kamp, M. W.; Mulholland, A. J. QM/MM Simulations as an Assay for Carbapenemase Activity in Class A β-Lactamases. *Chem. Commun.* **2014**, *50* (94), 14736–14739. https://doi.org/10.1039/C4CC06495J.

(29) Hirvonen, V. H. A.; Hammond, K.; Chudyk, E. I.; Limb, M. A. L.; Spencer, J.; Mulholland, A. J.; van der Kamp, M. W. An Efficient Computational Assay for β-Lactam Antibiotic Breakdown by Class A β-Lactamases. *J. Chem. Inf. Model.* **2019**, *59* (8), 3365–3369. https://doi.org/10.1021/acs.jcim.9b00442.

(30) Jabeen, H.; Beer, M.; Spencer, J.; van der Kamp, M. W.; Bunzel, H. A.; Mulholland, A. J. Electric Fields Are a Key Determinant of Carbapenemase Activity in Class A β-Lactamases. *ACS Catal.* **2024**, *14* (9), 7166–7172. https://doi.org/10.1021/acscatal.3c05302.

(31) Roux, B. The Calculation of the Potential of Mean Force Using Computer Simulations. *Comput. Phys. Commun.* **1995**, *91* (1–3), 275–282. https://doi.org/10.1016/0010-4655(95)00053-I.

(32) Grossfield, A. WHAM: the weighted histogram analysis method, version 2.0.10, http://membrane.urmc.rochester.edu/wordpress/?page_id=126.

(33) Marcos-Alcalde, I.; Setoain, J.; Mendieta-Moreno, J. I.; Mendieta, J.; Gómez-Puertas, P. MEPSA: Minimum Energy Pathway Analysis for Energy Landscapes. *Bioinformatics* **2015**, *31* (23), 3853–3855. https://doi.org/10.1093/bioinformatics/btv453.

(34) Mack, A. R.; Barnes, M. D.; Taracila, M. A.; Hujer, A. M.; Hujer, K. M.; Cabot, G.; Feldgarden, M.; Haft, D. H.; Klimke, W.; Van Den Akker, F.; Vila, A. J.; Smania, A.; Haider, S.; Papp-Wallace, K. M.; Bradford, P. A.; Rossolini, G. M.; Docquier, J. D.; Frère, J. M.; Galleni, M.; Hanson, N. D.; Oliver, A.; Plésiat, P.; Poirel, L.; Nordmann, P.; Palzkill, T. G.; Jacoby, G. A.; Bush, K.; Bonomo, R. A. A Standard Numbering Scheme for Class C β-Lactamases. *Antimicrob. Agents Chemother.* **2020**, *64* (3), 10.1128/aac.01841-19. https://doi.org/10.1128/AAC.01841-19.

(35) Tripathi, R.; Nair, N. N. Thermodynamic and Kinetic Stabilities of Active Site Protonation States of Class C β-Lactamase. *J. Phys. Chem. B* **2012**, *116* (16), 4741–4753. https://doi.org/10.1021/jp212186q.

(36) Adediran, S. A.; Pratt, R. F. β-Secondary and Solvent Deuterium Kinetic Isotope Effects on Catalysis by the Streptomyces R61 DD-Peptidase: Comparisons with a Structurally Similar Class C β-Lactamase. *Biochemistry* **1999**, *38* (5), 1469–1477. https://doi.org/10.1021/bi982308x.

(37) Chudyk, E. I.; Beer, M.; Limb, M. A. L.; Jones, C. A.; Spencer, J.; van der Kamp, M. W.; Mulholland, A. J. QM/MM Simulations Reveal the Determinants of Carbapenemase Activity in Class A β-Lactamases. *ACS Infect. Dis.* **2022**, *8* (8), 1521–1532. https://doi.org/10.1021/acsinfecdis.2c00152.

(38) Powers, R. A.; Caselli, E.; Focia, P. J.; Prati, F.; Shoichet, B. K. Structures of Ceftazidime and Its Transition-State Analogue in Complex with AmpC β-Lactamase: Implications for Resistance Mutations and Inhibitor Design. *Biochemistry* **2001**, *40* (31), 9207–9214. https://doi.org/10.1021/bi0109358.

(39) Gonzalez Leiza, M.; Perez-Diaz, J. C.; Ayala, J.; Casellas, J. M.; Martinez-Beltran,

J.; Bush, K.; Baquero, F. Gene Sequence and Biochemical Characterization of FOX-1 from Klebsiella Pneumoniae, a New AmpC-Type Plasmid-Mediated Beta-Lactamase with Two Molecular Variants. *Antimicrob. Agents Chemother.* **1994**, *38* (9), 2150–2157. https://doi.org/10.1128/AAC.38.9.2150.

(40) Knott-Hunziker, V.; Petursson, S.; Jayatilake, G. S.; Waley, S. G.; Jaurin, B.; Grundström, T. Active Sites of β-Lactamases. The Chromosomal β-Lactamases of Pseudomonas Aeruginosa and Escherichia Coli. *Biochem. J.* **1982**, *201* (3), 621–627. https://doi.org/10.1042/bj2010621.

(41) Roth, T. A.; Minasov, G.; Morandi, S.; Prati, F.; Shoichet, B. K. Thermodynamic Cycle Analysis and Inhibitor Design against Beta-Lactamase. *Biochemistry* **2003**, *42* (49), 14483–14491. https://doi.org/10.1021/bi035054a.

(42) Hirvonen, V. H. A.; Weizmann, T. M.; Mulholland, A. J.; Spencer, J.; van der Kamp, M. W. Multiscale Simulations Identify Origins of Differential Carbapenem Hydrolysis by the OXA-48 β-Lactamase. *ACS Catal.* **2022**, *12* (8), 4534–4544. https://doi.org/10.1021/acscatal.1c05694.

(43) B., V. S.; Dasantila, G.; Bruce, G.; Maxim, S.; R., K. J.; Shahriar, M.; A., L. S. Mutational Replacement of Leu-293 in the Class C Enterobacter Cloacae P99 β-Lactamase Confers Increased MIC of Cefepime. *Antimicrob. Agents Chemother.* **2002**, *46* (6), 1966–1970. https://doi.org/10.1128/aac.46.6.1966-1970.2002.

(44) Vijayakumar, S.; Ravishanker, G.; Pratt, R. F.; Beveridge, D. L. Molecular Dynamics Simulation of a Class A .Beta.-Lactamase: Structural and Mechanistic Implications. *J. Am. Chem. Soc.* **1995**, *117* (6), 1722–1730. https://doi.org/10.1021/ja00111a008.